

Exploiting the High Dimensionality of Polarimetric Interferometric Synthetic Aperture Radar Observations

Robert Riley
rriley@sandia.gov

R. Derek West
rdwest@sandia.gov

This work was supported by the Laboratory Directed Research and Development program at Sandia National Laboratories. Sandia National Laboratories is a multimission laboratory managed and operated by National Technology and Engineering Solutions of Sandia LLC, a wholly owned subsidiary of Honeywell International Inc. for the U.S. Department of Energy's National Nuclear Security Administration under contract DE-NA0003525.

Presentation Outline

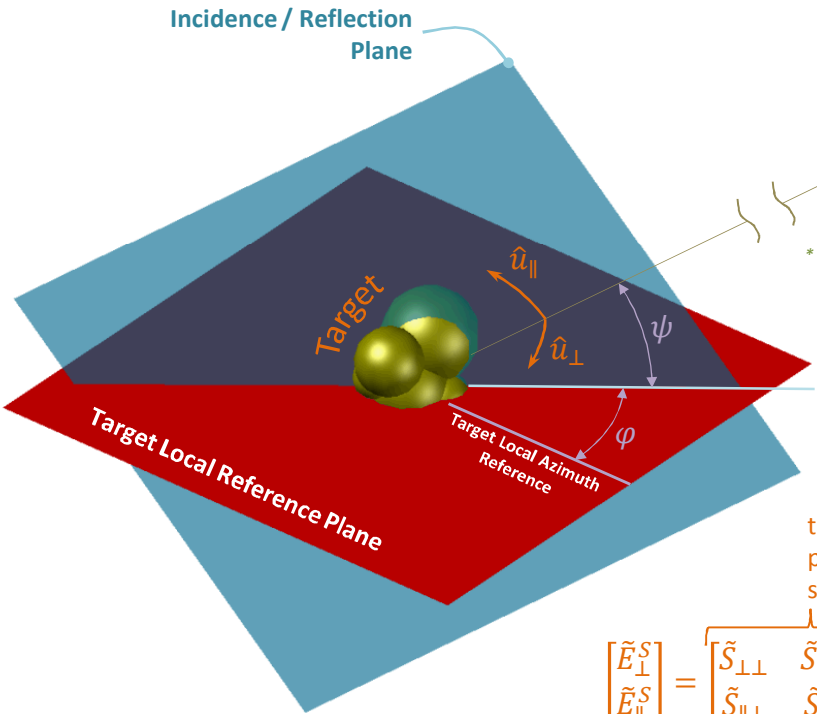
- Polarimetric SAR Background
- Polarization States and Canonical Scatterers
- Polarimetric SAR Decompositions
- Temporal Coherence / Change Detection
- Application: Polarimetric SAR Change Discrimination

POLARIMETRIC SAR BACKGROUND

Polarimetric Radar (Monostatic)

Targets do not only reflect in polarization that was incident

Complete understanding of scattering interface requires polarimetric observations



planar far-field approximation

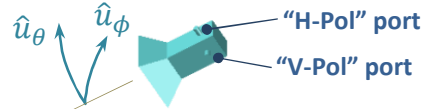
$$\hat{v} \leftrightarrow \hat{h} \leftrightarrow \hat{u}_\phi$$

$$\hat{u}_\perp \leftrightarrow \hat{h} \leftrightarrow \hat{u}_\phi$$

$$\hat{u}_\parallel \leftrightarrow \hat{v} \leftrightarrow \hat{u}_\theta$$

* antenna must be roll-axis stabilized relative to target local reference plane

Radar Antenna



$$\begin{matrix} \text{H-Pol Port} \\ \text{V-Pol Port} \end{matrix} \begin{bmatrix} \tilde{E}_\phi^R \\ \tilde{E}_\theta^R \end{bmatrix} = \frac{e^{-2jk_r r}}{r^2} \underbrace{\begin{bmatrix} \tilde{S}_{\phi\phi} & \tilde{S}_{\phi\theta} \\ \tilde{S}_{\theta\phi} & \tilde{S}_{\theta\theta} \end{bmatrix}}_{\text{free-space propagation, far-field approximation}} \underbrace{\begin{bmatrix} \tilde{S}_{\phi\phi} & \tilde{S}_{\phi\theta} \\ \tilde{S}_{\theta\phi} & \tilde{S}_{\theta\theta} \end{bmatrix}}_{\text{target backscatter influence on receive measurement}} \begin{bmatrix} \tilde{E}_\phi^T \\ \tilde{E}_\theta^T \end{bmatrix}$$

After calibration and far-field assumptions, the radar measurements of target backscatter are represented as...

$$\begin{bmatrix} \tilde{S}_{HH} & \tilde{S}_{HV} \\ \tilde{S}_{VH} & \tilde{S}_{VV} \end{bmatrix}_{(\varphi, \psi)}$$

Order of polarization subscripts follows scattered / incident order

target's geometry & polarization dependent scattering matrix

$$\begin{bmatrix} \tilde{E}_\perp^S \\ \tilde{E}_\parallel^S \end{bmatrix} = \begin{bmatrix} \tilde{S}_{\perp\perp} & \tilde{S}_{\perp\parallel} \\ \tilde{S}_{\parallel\perp} & \tilde{S}_{\parallel\parallel} \end{bmatrix}_{(\varphi, \psi)} \begin{bmatrix} \tilde{E}_\perp^I \\ \tilde{E}_\parallel^I \end{bmatrix}$$

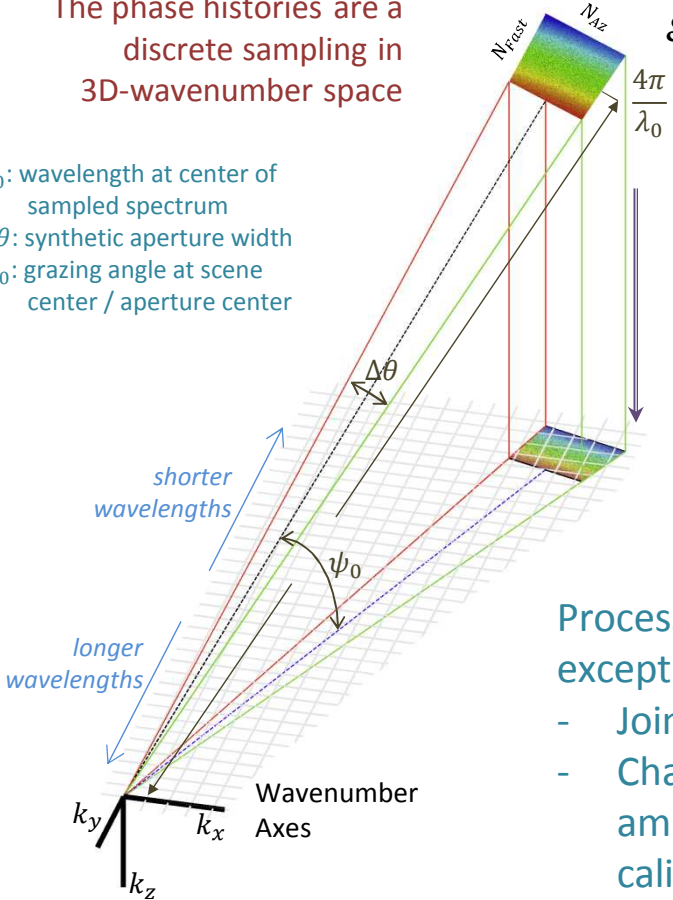
back-scattered E-Field

incident E-Field

Polarimetric Spotlight SAR

The phase histories are a discrete sampling in 3D-wavenumber space

λ_0 : wavelength at center of sampled spectrum
 $\Delta\theta$: synthetic aperture width
 ψ_0 : grazing angle at scene center / aperture center



At each phase history spectral sample location (f, a) :

$$\mathcal{S}(k_x, a, k_y, f) = \begin{bmatrix} \tilde{\mathcal{S}}_{HH} & \tilde{\mathcal{S}}_{HV} \\ \tilde{\mathcal{S}}_{VH} & \tilde{\mathcal{S}}_{VV} \end{bmatrix}_{(f, a)}$$

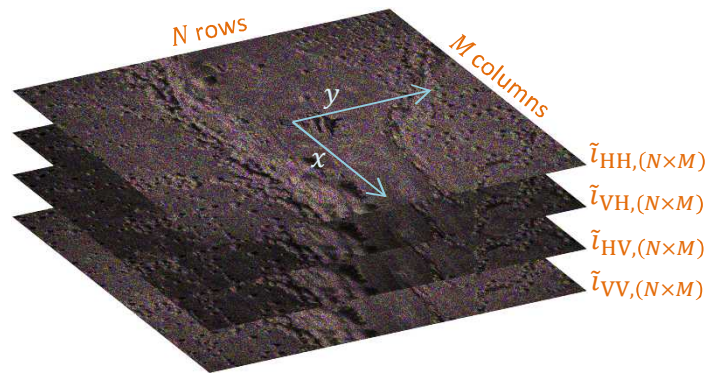
$$\mathcal{S}(k_x, k_y) \rightarrow \mathcal{S}(x, y)$$

SAR 2D Image Formation

Processing proceeds as usual, except we now require...

- Joint autofocus
- Channel-to-channel amplitude and phase calibration

Four Complex Image Channels

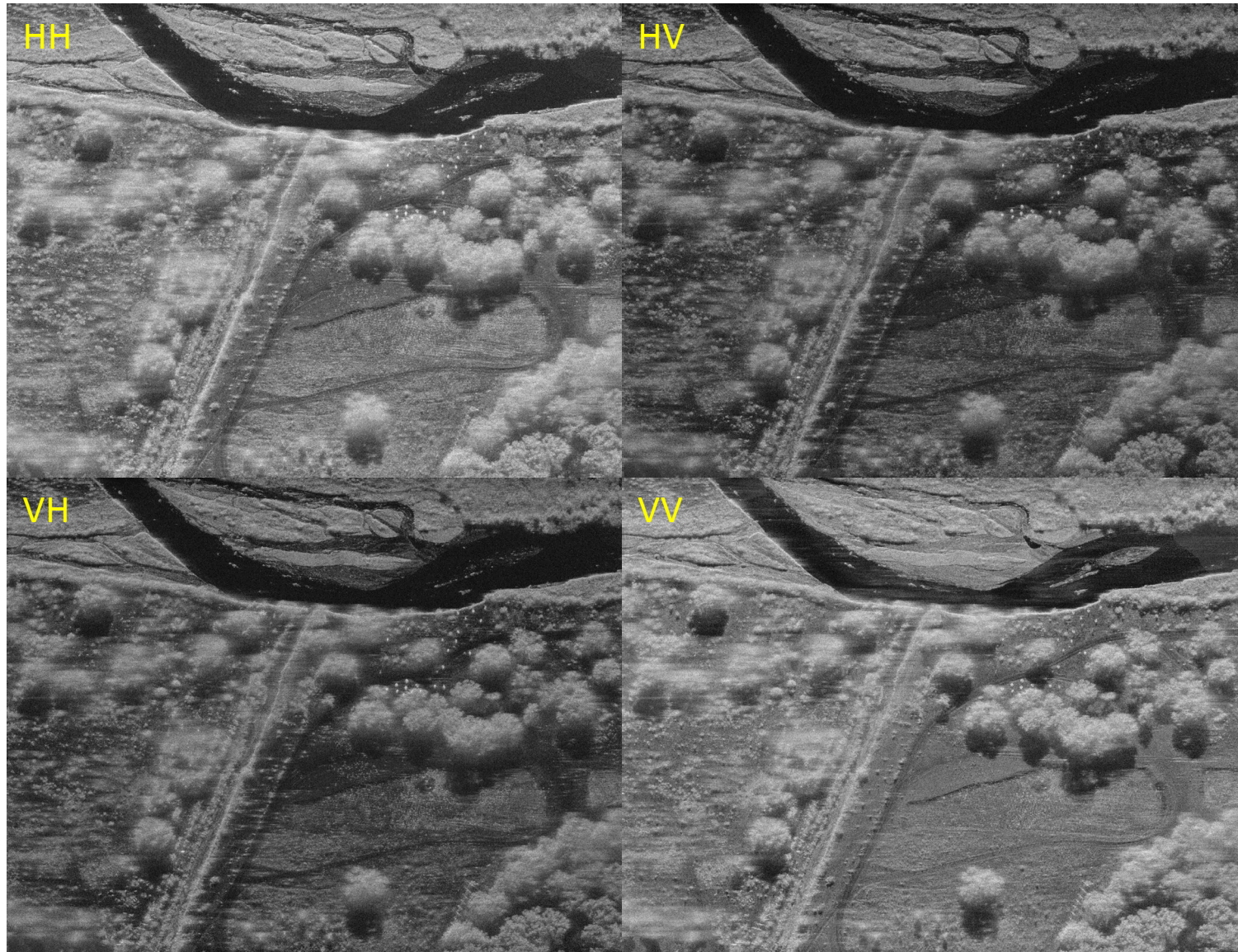


At each image pixel (n, m) :

$$\mathcal{S}(x_m, y_n) = \begin{bmatrix} \tilde{\mathcal{S}}_{HH} & \tilde{\mathcal{S}}_{HV} \\ \tilde{\mathcal{S}}_{VH} & \tilde{\mathcal{S}}_{VV} \end{bmatrix}_{(n, m)}$$

- 7** degrees of freedom in each raw backscatter observation:
- 4 in magnitude
- 3 in relative phases

Example: Polarimetric SAR Magnitude Images



Chief value in polarimetric SAR is not in visual comparison of individual channel backscatter intensity maps!

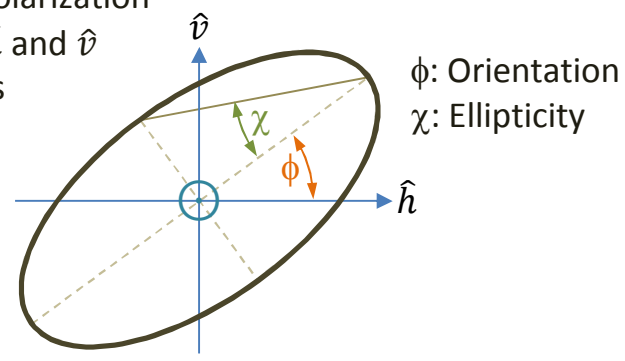
Some Immediate Value Adds of Polarimetric SAR

- Pixel-level assessment of the phenomenological nature of point and distributed scattering targets
- Robust inference of scattering mechanisms
- Supervised and unsupervised land cover classification
- Higher achievable coherence
- Increased flexibility in change-type discrimination

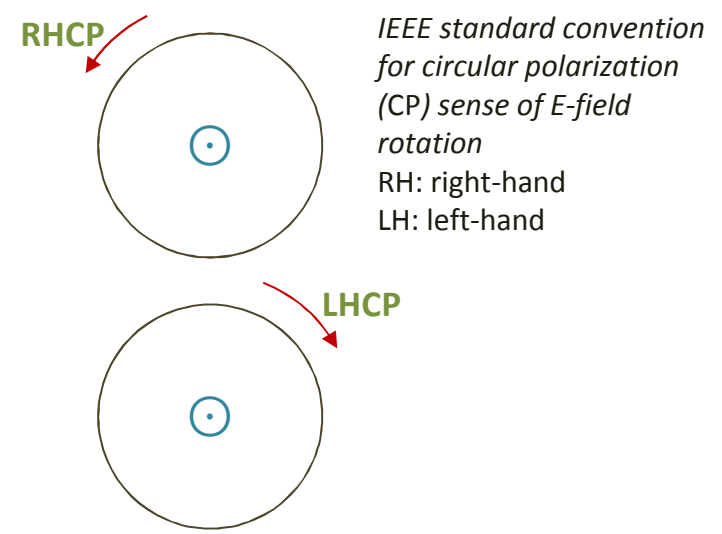
POLARIZATION STATES AND CANONICAL SCATTERERS

Scattering Polarization States

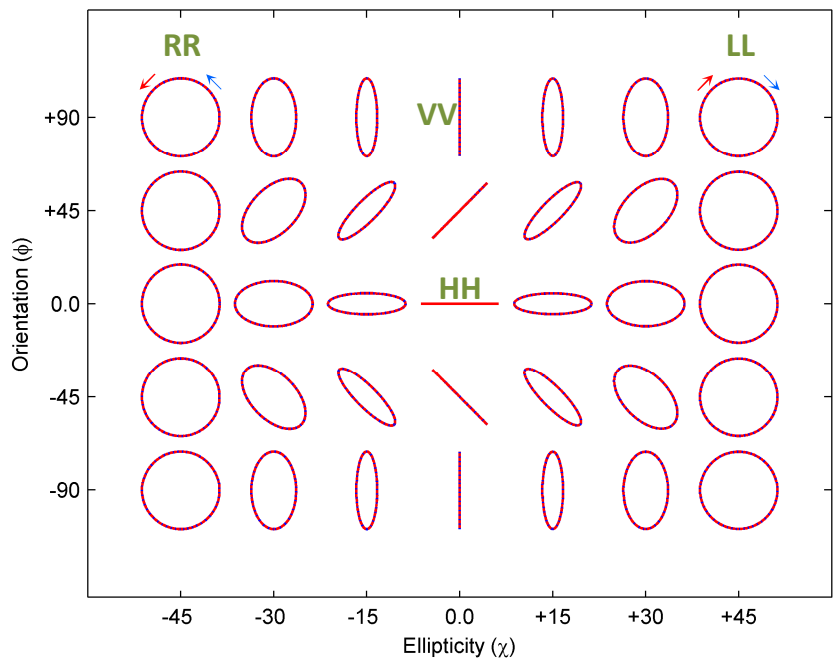
E-field elliptical polarization locus relative to \hat{h} and \hat{v} polarization bases



Propagation towards viewer indicated by \odot

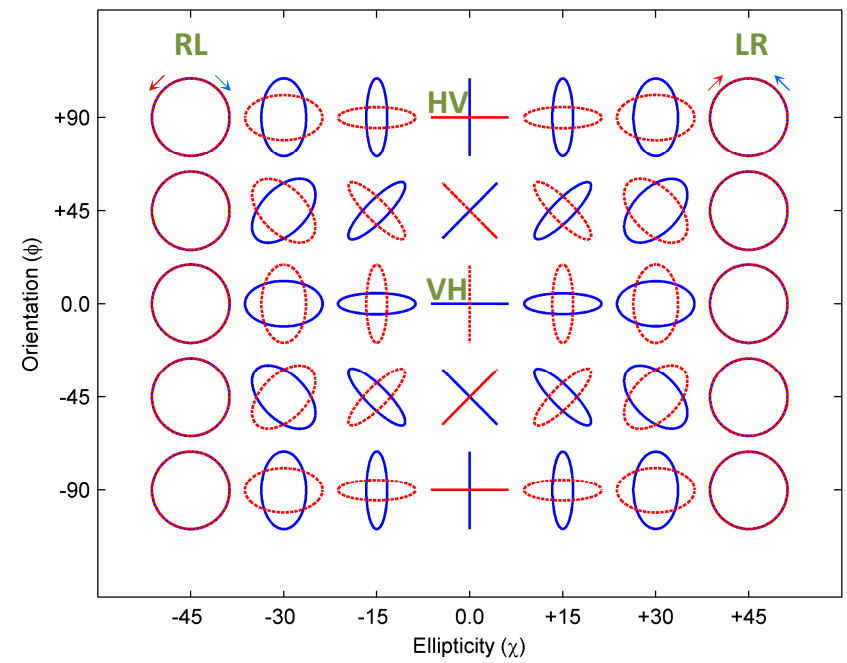


Co-Pol Scattering States



Incident ——— blue
Scattered ——— red

Cross-Pol Scattering States



Change of Polarization Bases and Consimilarity Transform

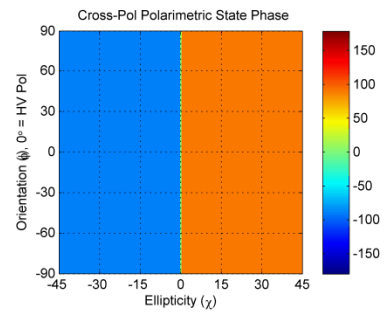
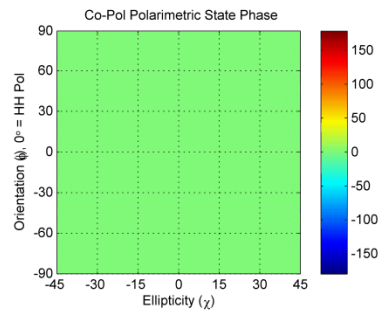
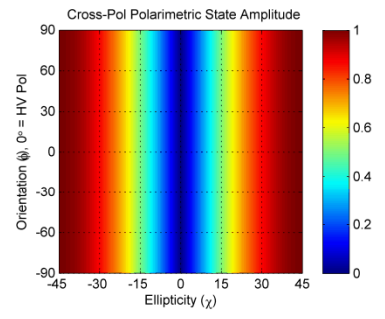
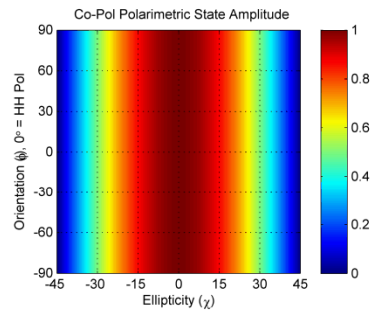
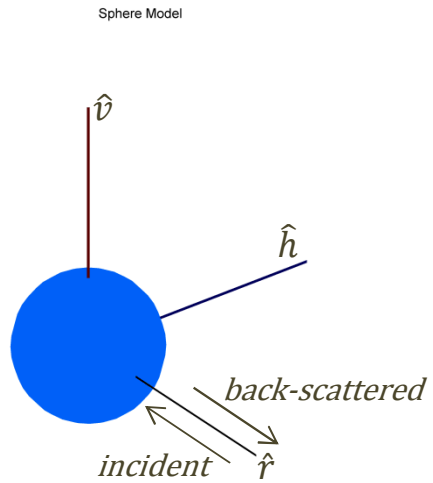
- The S matrix can be transformed to represent scattering due to any other pair of orthogonal bases, including elliptical and circular
- The unitary consimilarity transform can be utilized to achieve any new orthogonal basis set from coherent polarimetric measurements:

$$\mathbf{S}_{(\hat{u}, \hat{u}_\perp)} = \mathbf{U}_2(\phi, \chi)^T \mathbf{S}_{(\hat{x}, \hat{y})} \mathbf{U}_2(\phi, \chi)$$
$$\mathbf{U}_2(\phi, \chi) = \begin{bmatrix} \cos \phi & -\sin \phi \\ \sin \phi & \cos \phi \end{bmatrix} \begin{bmatrix} \cos \chi & j \sin \chi \\ j \sin \chi & \cos \chi \end{bmatrix}$$

- Each S matrix has a 2D response mapping into the orientation / ellipticity parameter space (polarization states)
- The structure of this mapping is unique for canonical scattering mechanisms
- Polarized scatterers can be decomposed into superpositions of canonical mechanisms

Canonical Scatterers: Sphere

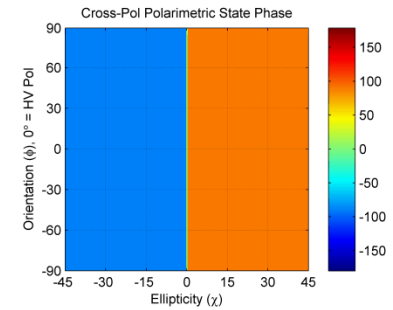
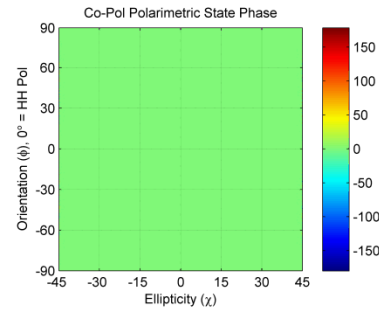
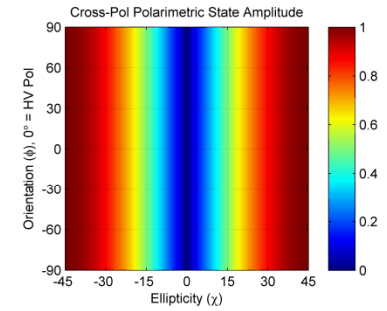
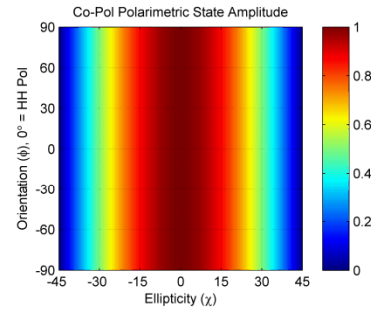
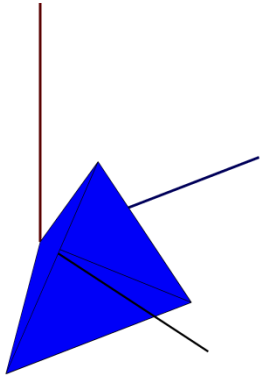
$$S_{\text{sphere},(\hat{v},\hat{h})} \propto \begin{bmatrix} 1 & 0 \\ 0 & 1 \end{bmatrix}$$



Canonical Scatterers: Trihedral

$$\mathbf{S}_{\text{trihedral},(\hat{v},\hat{h})} \propto \begin{bmatrix} 1 & 0 \\ 0 & 1 \end{bmatrix} \quad \text{at boresight, back-scatter response is orientation independent!}$$

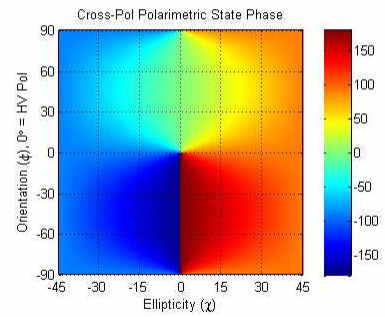
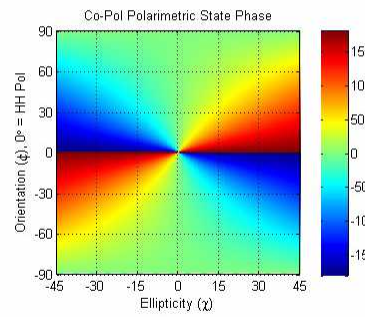
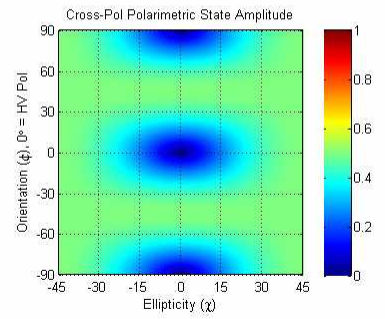
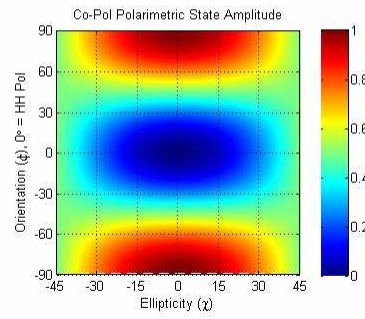
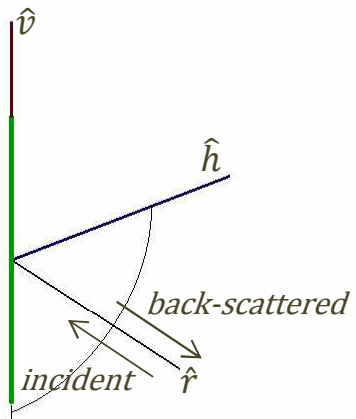
Trihedral Model



Canonical Scatterers: Oriented Thin Cylinder

$$S_{\text{dipole},(\hat{v},\hat{h})} \propto \begin{bmatrix} \cos^2 \theta & \frac{1}{2} \sin 2\theta \\ \frac{1}{2} \sin 2\theta & \sin^2 \theta \end{bmatrix}$$

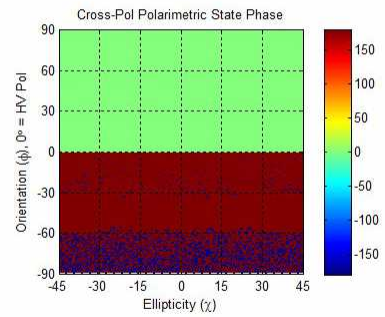
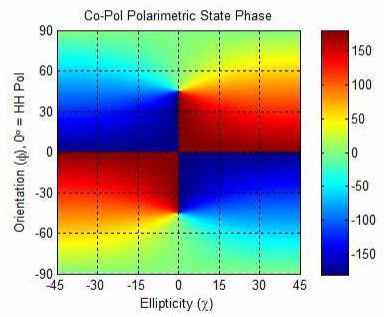
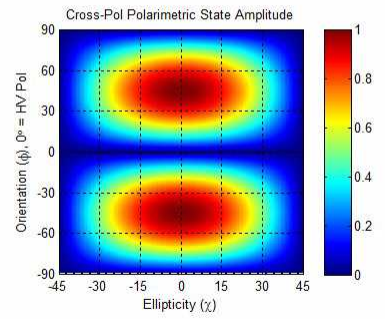
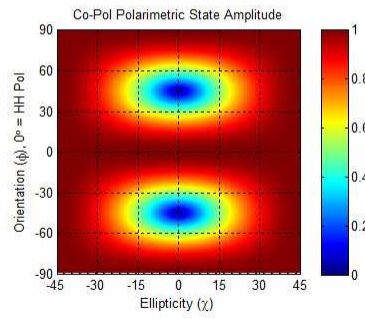
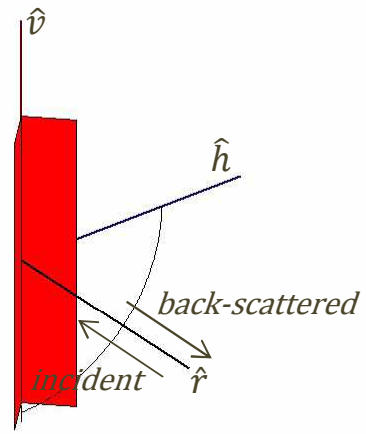
Dipole Model, $\theta = -90.0^\circ$



Canonical Scatterers: Oriented Dihedral

$$S_{\text{dihedral},(\hat{v},\hat{h})} \propto \begin{bmatrix} \cos 2\theta & \sin 2\theta \\ \sin 2\theta & -\cos 2\theta \end{bmatrix}$$

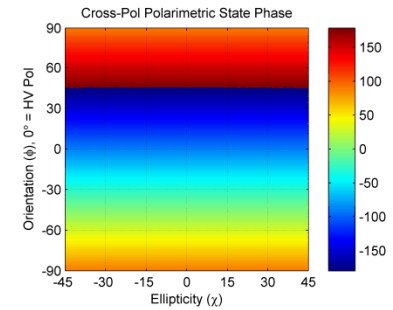
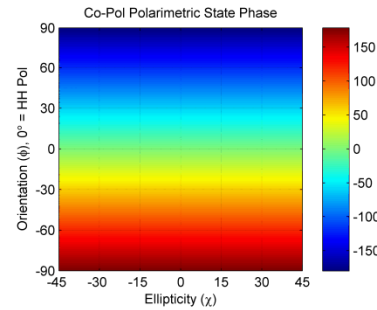
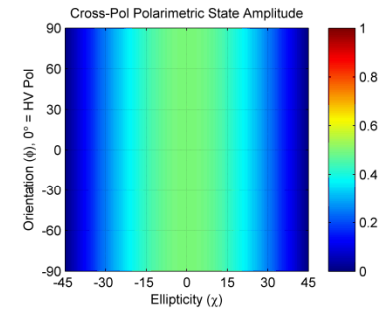
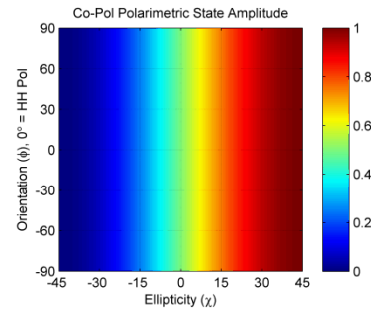
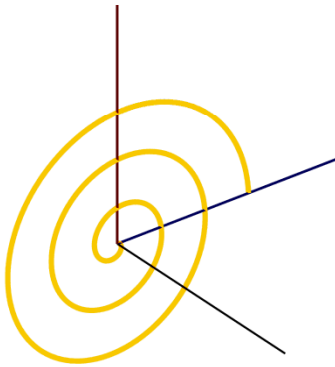
Dihedral Model, $\theta = -90.0^\circ$



Canonical Scatterers: Right-Hand Spiral / Helical

$$\mathcal{S}_{r.\text{spiral},(\hat{v},\hat{h})} \propto \frac{1}{2} \begin{bmatrix} 1 & -j \\ -j & -1 \end{bmatrix}$$

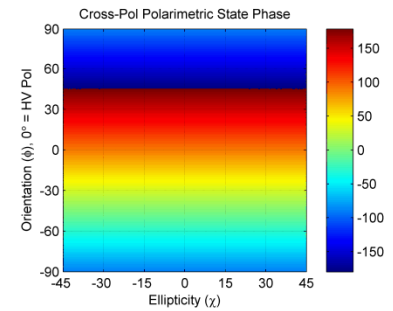
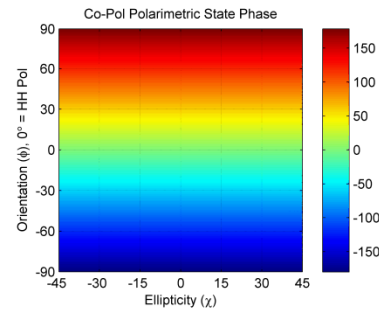
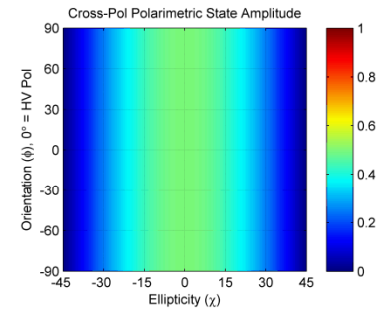
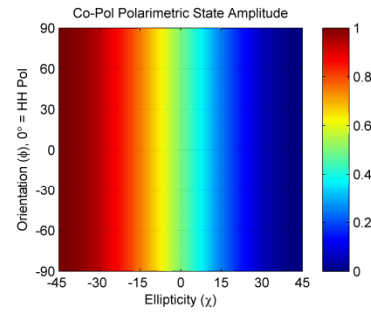
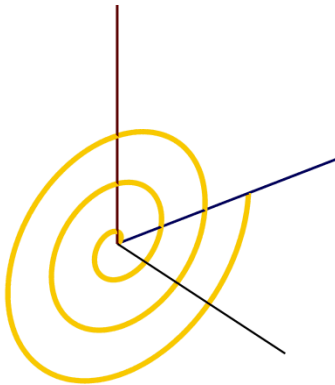
Right Helix Model



Canonical Scatterers: Left-Hand Spiral / Helical

$$\mathbf{S}_{l.\text{spiral},(\hat{v},\hat{h})} \propto \frac{1}{2} \begin{bmatrix} 1 & j \\ j & -1 \end{bmatrix}$$

Left Helix Model



POLARIMETRIC SAR DECOMPOSITIONS

Pauli Feature Vector

The Pauli decomposition is a basic polarimetric decomposition; more sophisticated & robust decompositions are built on this foundation

Scattering matrix for each pixel is re-cast into the Pauli feature vector, \bar{k} .

Each row of the vector provides a general inference about the reflections observed at a pixel:

$$\bar{k} = \frac{1}{\sqrt{2}} \begin{bmatrix} \tilde{S}_{HH} + \tilde{S}_{VV} \\ \tilde{S}_{HH} - \tilde{S}_{VV} \\ 2\tilde{S}_{CX} \end{bmatrix}$$

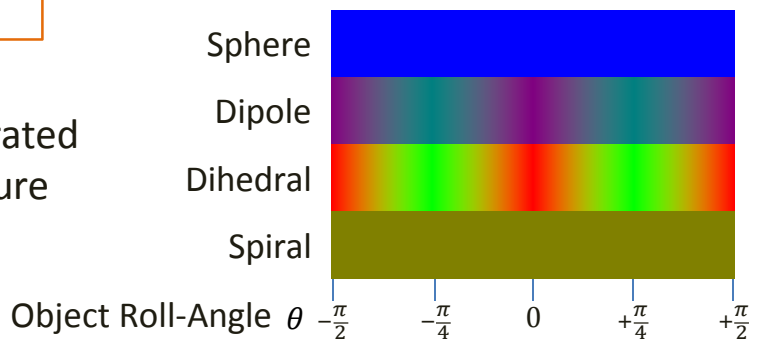
→ Odd bounce, surface
→ Even bounce, 0° / 90° di-plane
→ Even bounce, ±45° di-plane

Monostatic, reflection symmetry $\rightarrow \langle \tilde{S}_{HV} \rangle = \langle \tilde{S}_{VH} \rangle$
 Cross-pol element created by mean of independent cross-pol measures:
 $\tilde{S}_{CX} = (\tilde{S}_{HV} + \tilde{S}_{VH})/2$

An RGB composite image can be generated from the magnitudes of the Pauli feature vector representation

$$\bar{k}_{\text{sphere}} \propto \sqrt{2} \begin{bmatrix} 1 \\ 0 \\ 0 \end{bmatrix} \quad \bar{k}_{\text{spiral}} \propto \frac{\sqrt{2}}{2} \begin{bmatrix} 0 \\ 1 \\ \mp j \end{bmatrix}$$

$$\bar{k}_{\text{dipole}} \propto \frac{\sqrt{2}}{2} \begin{bmatrix} 1 \\ \cos 2\theta \\ \sin 2\theta \end{bmatrix} \quad \bar{k}_{\text{dihedral}} \propto \sqrt{2} \begin{bmatrix} 0 \\ \cos 2\theta \\ \sin 2\theta \end{bmatrix}$$



Polarimetric Coherence Matrix

Pauli feature vector does not directly utilize all of the magnitude and phase relationships between co-pol and cross-pol measurements

Many advanced polarimetric decompositions make use of the polarimetric coherence matrix (\mathbf{T}_3), which is the outer product of the Pauli feature vector and its conjugate

$$\mathbf{T}_3 = \bar{\mathbf{k}} \otimes \bar{\mathbf{k}}^* = \bar{\mathbf{k}}\bar{\mathbf{k}}^H$$

$$\mathbf{T}_3 = \frac{1}{2} \begin{bmatrix} |\tilde{S}_{HH} + \tilde{S}_{VV}|^2 & (\tilde{S}_{HH} + \tilde{S}_{VV})(\tilde{S}_{HH} - \tilde{S}_{VV})^* & 2(\tilde{S}_{HH} + \tilde{S}_{VV})\tilde{S}_{CX}^* \\ (\tilde{S}_{HH} - \tilde{S}_{VV})(\tilde{S}_{HH} + \tilde{S}_{VV})^* & |\tilde{S}_{HH} - \tilde{S}_{VV}|^2 & 2(\tilde{S}_{HH} - \tilde{S}_{VV})\tilde{S}_{CX}^* \\ 2\tilde{S}_{CX}(\tilde{S}_{HH} + \tilde{S}_{VV})^* & 2\tilde{S}_{CX}(\tilde{S}_{HH} - \tilde{S}_{VV})^* & 4|\tilde{S}_{CX}|^2 \end{bmatrix}$$

$$\mathbf{T}_{3,\text{sphere}} \propto \frac{1}{2} \begin{bmatrix} 1 & 0 & 0 \\ 0 & 0 & 0 \\ 0 & 0 & 0 \end{bmatrix}$$

$$\mathbf{T}_{3,\text{spiral}} \propto \frac{1}{4} \begin{bmatrix} 0 & 0 & 0 \\ 0 & 1 & \mp j \\ 0 & \pm j & 1 \end{bmatrix}$$

$$\mathbf{T}_{3,\text{dipole}} \propto \frac{1}{2} \begin{bmatrix} 1 & \cos 2\theta & \sin 2\theta \\ \cos 2\theta & \cos^2 2\theta & \cos 2\theta \sin 2\theta \\ \sin 2\theta & \cos 2\theta \sin 2\theta & 2 \sin 2\theta \end{bmatrix}$$

$$\mathbf{T}_{3,\text{dihedral}} \propto 2 \begin{bmatrix} 0 & 0 & 0 \\ 0 & \cos^2 2\theta & \cos 2\theta \sin 2\theta \\ 0 & \cos 2\theta \sin 2\theta & \sin^2 2\theta \end{bmatrix}$$

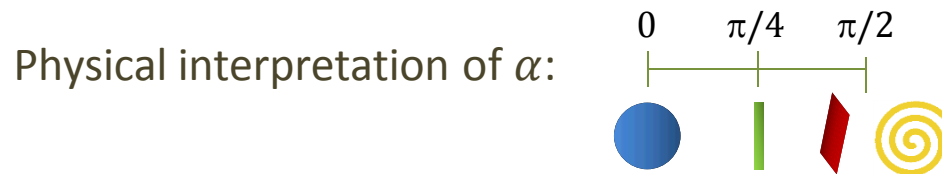
H/A/ α Decomposition

Polarimetric coherency matrix, T_3 , can be decomposed into three real non-negative eigenvalues (λ) and corresponding unit complex eigenvectors (\bar{u})

Each eigenvector / eigenvalue represents a polarized target scattering mechanism and its contribution to the total observed backscatter.

Each eigenvector can be parameterized into five angles ($\alpha, \beta, \gamma, \delta, \phi$)

The α angle parameter has a correspondence to the underlying scattering mechanism



The dominance of the strongest of the three supported scattering mechanisms can be equated to the entropy (H) of the eigenvalues.

An additional parameter referred to as the polarimetric anisotropy (A) indicates the strength of the lesser two of the three supported scattering mechanisms.

The H/A/ α parameters are roll-invariant

The H/A/ α Decomposition Formulation

eigendecomposition of coherency matrix

$$\mathbf{T}_3 = \mathbf{U}_3 \mathbf{\Lambda} \mathbf{U}_3^{-1} = \sum_{i=1}^3 \lambda_i \bar{\mathbf{u}}_i \cdot \bar{\mathbf{u}}_i^H$$

$$\lambda_1 \geq \lambda_2 \geq \lambda_3$$

eigenvector parameterization

$$\bar{\mathbf{u}}_i = e^{j\phi_i} \begin{bmatrix} \cos \alpha_i \\ \sin \alpha_i \cos \beta_i e^{j\delta_i} \\ \sin \alpha_i \sin \beta_i e^{j\gamma_i} \end{bmatrix}$$

roll-invariant scattering mechanism parameter

$$\alpha_i = \cos^{-1} |\bar{\mathbf{u}}_{i,1}|$$

pseudo-probabilities of eigenvalues

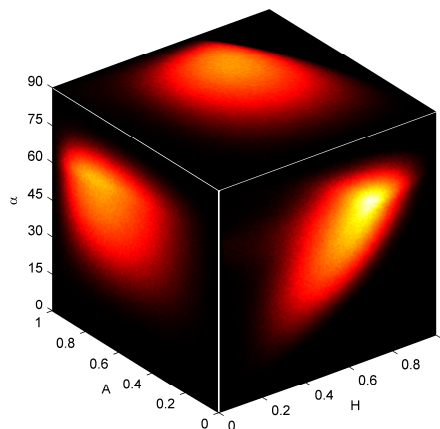
$$P_i = \frac{\lambda_i}{\sum_{k=1}^3 \lambda_k}$$

Entropy $H = - \sum_{k=1}^3 P_k \log_3 P_k$

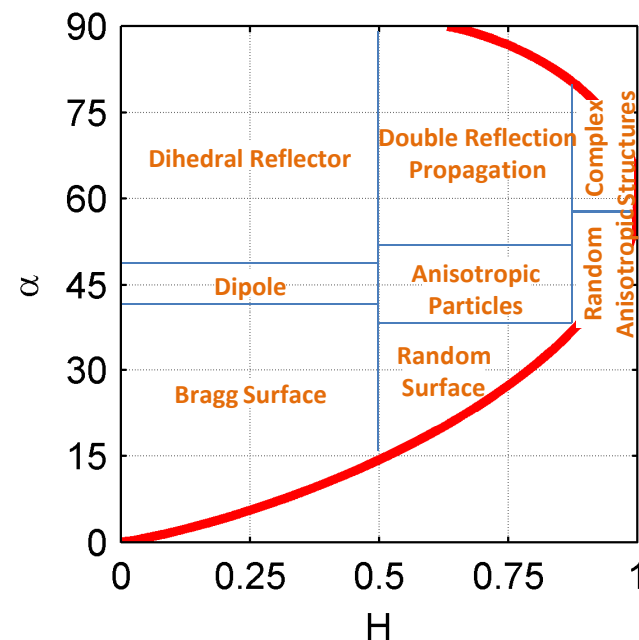
Anisotropy $A = \frac{\lambda_2 - \lambda_3}{\lambda_2 + \lambda_3}$

Mean roll-invariant scattering mechanism parameter $\bar{\alpha} = \sum_{k=1}^3 P_k \alpha_k$

* Total backscatter intensity is an additional independent parameter



Example 3D parameter space density plot



Yamaguchi / G4U Decomposition

The General Four-Component Scattering Power Decomposition with Unitary Transformation of Coherency Matrix (**G4U**) is the *state-of-the-art model-based* decomposition that fits the coherency matrix to contributions from four independent canonical scattering mechanisms.

$$\langle \mathbf{T}_3 \rangle = P_s \langle [\mathbf{T}_3] \rangle_{\text{surface}} + P_d \langle [\mathbf{T}_3] \rangle_{\text{double}} + P_v \langle [\mathbf{T}_3] \rangle_{\text{vol}} + P_c \langle [\mathbf{T}_3] \rangle_{\text{helix}}$$

$\langle \cdot \rangle$ is expectation operator, performed with spatial ensemble average

The four $[\mathbf{T}_3]_m$ are coherence models for the scattering mechanisms

$P_s, P_d, P_v,$ and P_c are the real expansion coefficients to be determined

G4U (c. 2013) advanced prior Yamaguchi (c. 2005) decomposition by removing dependence on orientation (i.e. roll invariance)

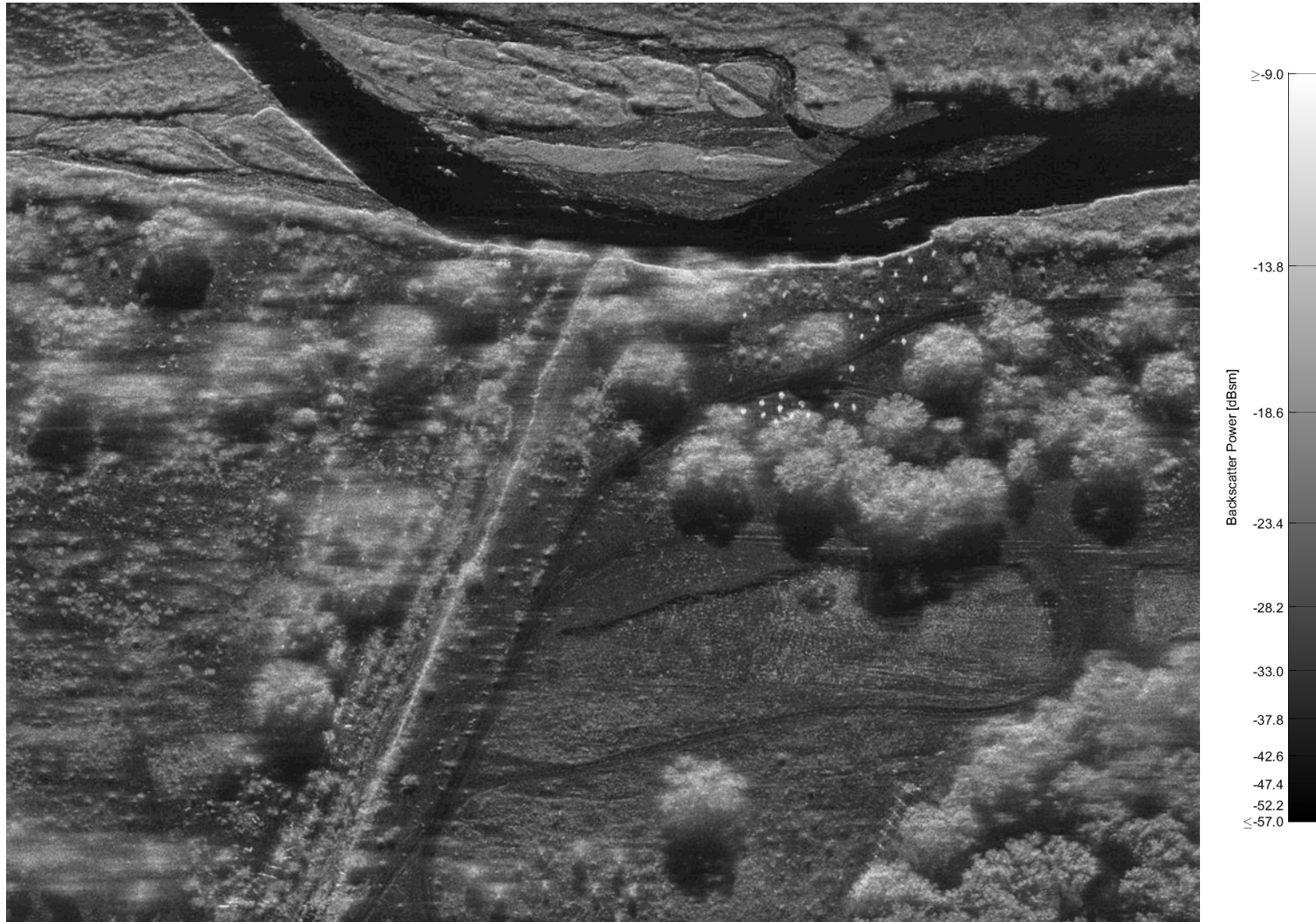
Y. Yamaguchi, et. al., "Four-component scattering model for polarimetric SAR image decomposition," *Geoscience and Remote Sensing, IEEE Transactions on*, vol. 43, no. 8, pp. 1699-1706, 2005.

J.S. Lee and T.L. Ainsworth, "The effect of orientation angle compensation on coherency matrix and polarimetric target decompositions," *Geoscience and Remote Sensing, IEEE Transactions on*, vol. 49, no. 1, pp. 53-64, 2011.

Y. Yamaguchi, et. al., "On complete model-based decomposition of polarimetric SAR coherency matrix data," *Geoscience and Remote Sensing, IEEE Transactions on*, vol. 52, no. 4, pp. 1991-2001, 2014.

Comparative Display Image Products

Span (Total Power) Image

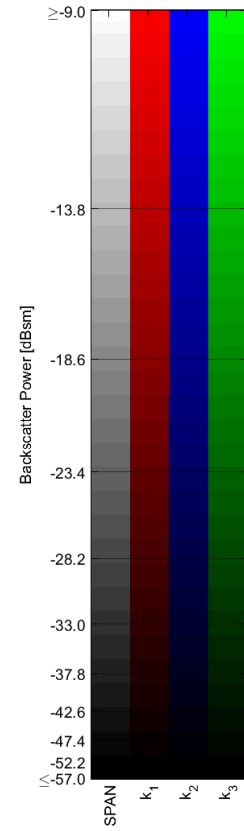
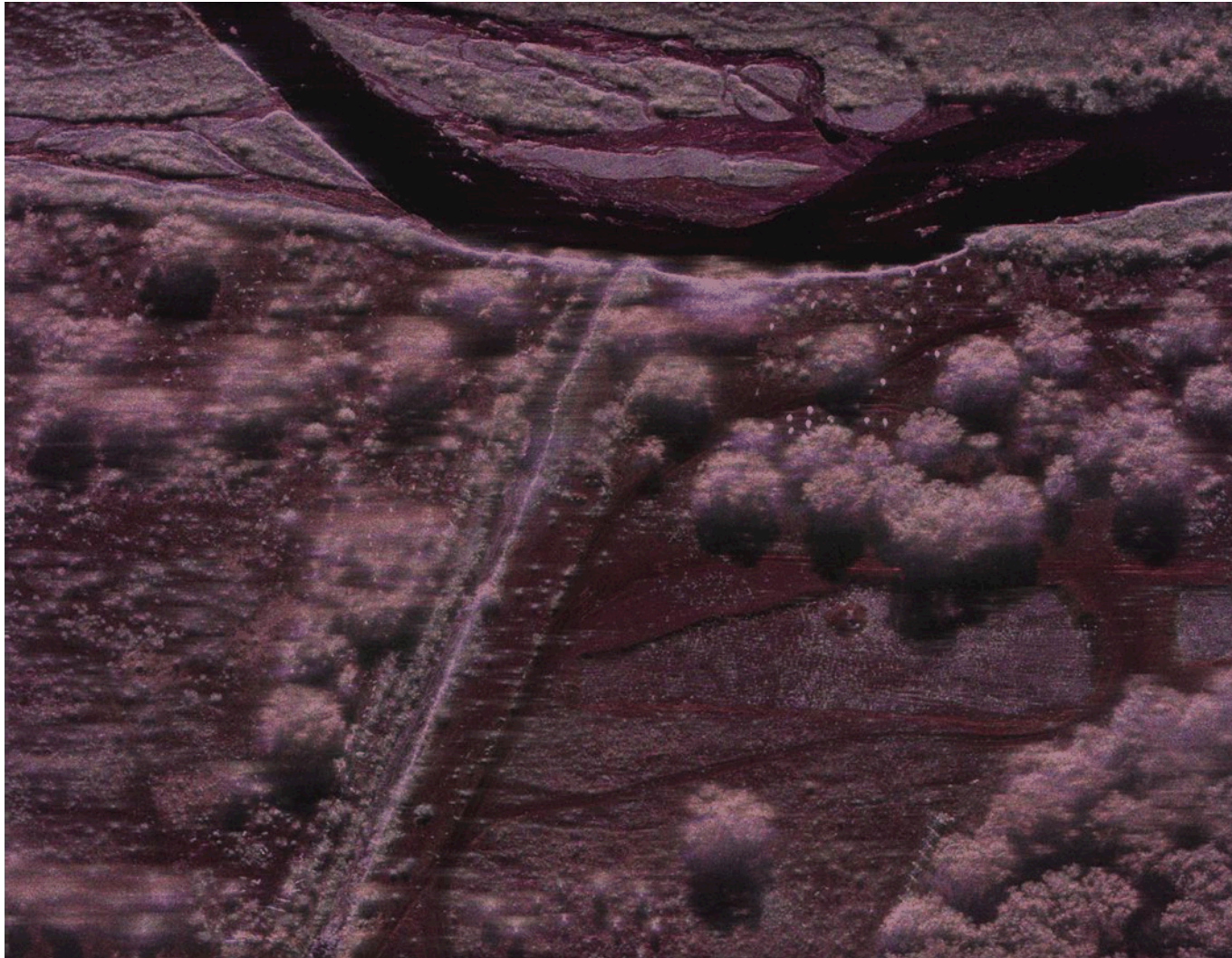


SNL FARAD X-Band SAR, imaged July 17, 2013

35.0° grazing, -89.9° squint, 0.1016m range resolution, 0.1117m azimuth resolution

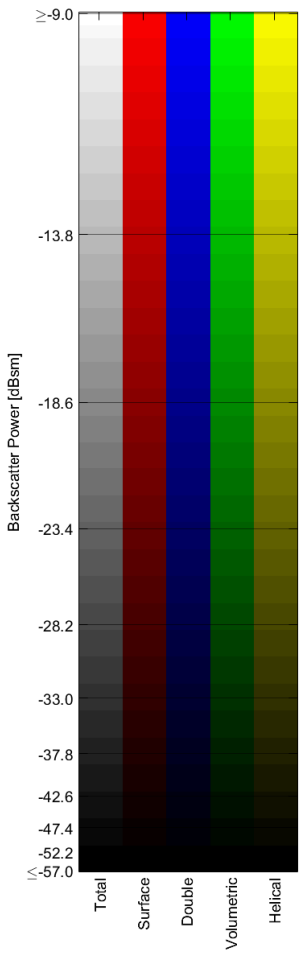
Comparative Display Image Products

Pauli Decomposition



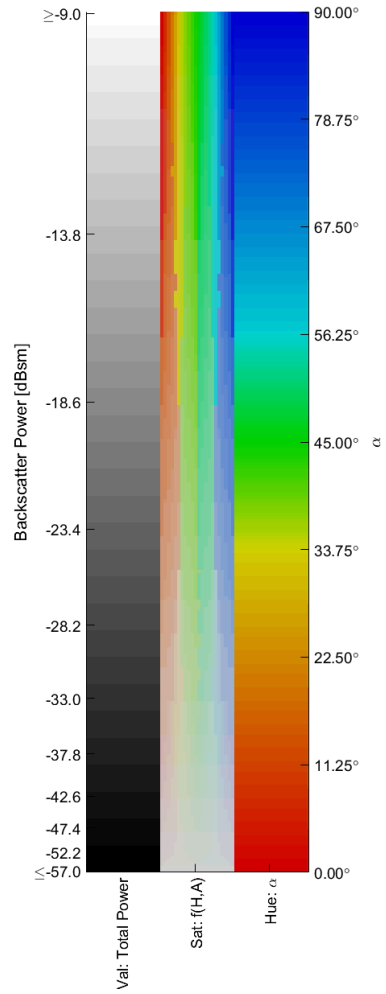
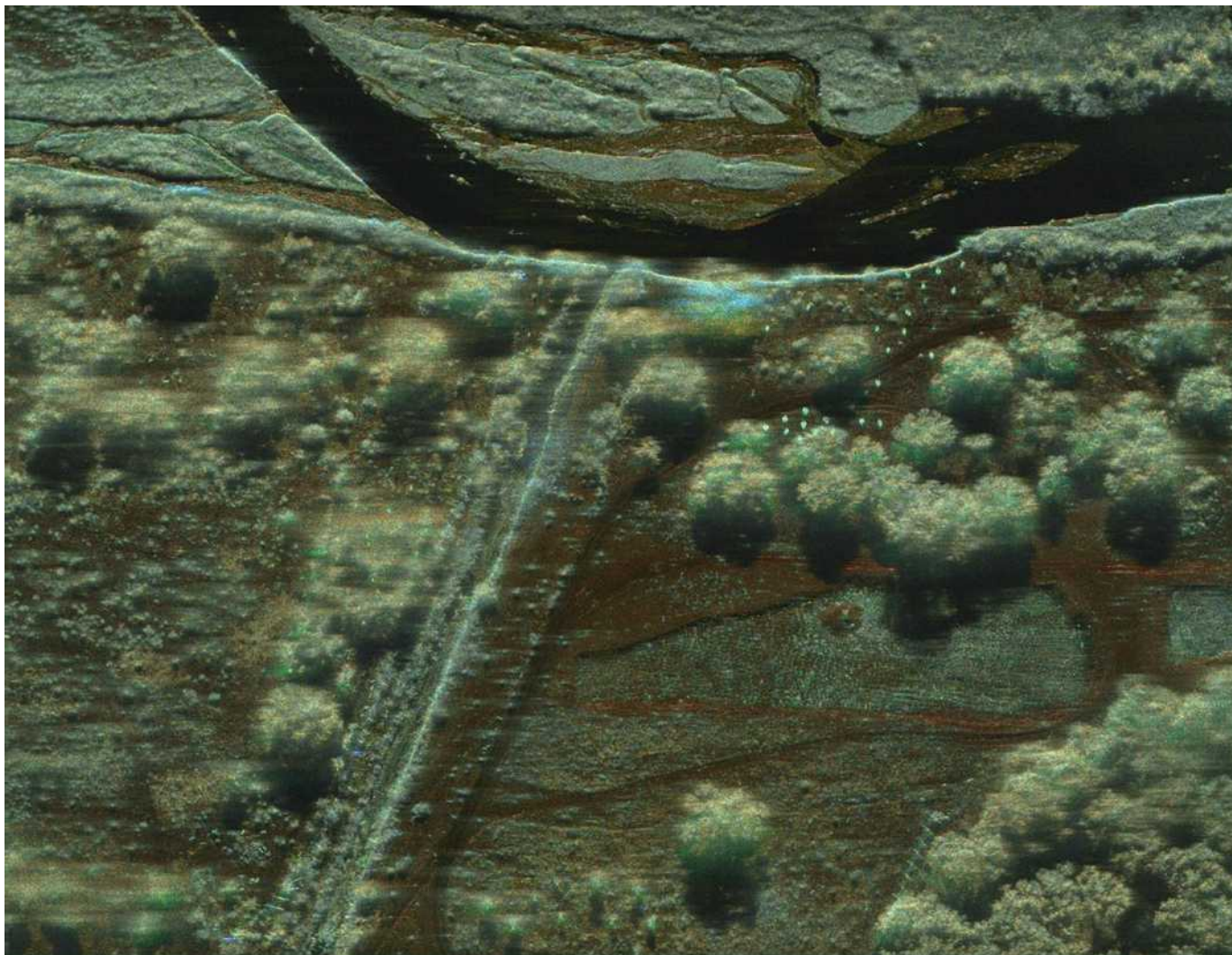
Comparative Display Image Products

G4U Decomposition



Comparative Display Image Products

H/A/ α Decomposition




TEMPORAL COHERENCE / CHANGE DETECTION

Polarimetric Interferometric Coherence

The standard expression for the estimate of complex coherence of an interferometric image pair $(\tilde{i}_1, \tilde{i}_2)$ is:

$$\tilde{\gamma} = \frac{\langle \tilde{i}_1 \tilde{i}_2^* \rangle}{\sqrt{\langle \tilde{i}_1 \tilde{i}_1^* \rangle \langle \tilde{i}_2 \tilde{i}_2^* \rangle}}, \quad 0 \leq |\tilde{\gamma}| \leq 1$$


CCD (coherent change detection) product is the display of this magnitude

The generalized polarimetric estimate for complex coherence:

$$\tilde{\gamma} = \frac{\bar{w}_1^H \mathbf{\Omega} \bar{w}_2}{\sqrt{(\bar{w}_1^H \mathbf{T}_1 \bar{w}_1)(\bar{w}_2^H \mathbf{T}_2 \bar{w}_2)}}, \quad 0 \leq |\tilde{\gamma}| \leq 1$$

$$\mathbf{T}_1 = \langle \bar{k}_1 \bar{k}_1^H \rangle, \quad \mathbf{T}_2 = \langle \bar{k}_2 \bar{k}_2^H \rangle, \quad \mathbf{\Omega} = \langle \bar{k}_1 \bar{k}_2^H \rangle$$

\bar{w}_1 and \bar{w}_2 are mechanism-related normalized complex weighting vectors
 There exists a closed form solution for a weight pair that optimizes coherence

Uses of polarimetric interferometry include DEM, DTM and subsidence analysis

Substantively higher coherence can typically be maintained, with correspondingly improved interferometric phase estimates

M. Preiss, D.A. Gray, and N.J.S. Stacy, "Detecting scene changes using synthetic aperture radar interferometry," *Geoscience and Remote Sensing, IEEE Transactions on*, vol. 44, no. 8, pp. 2041-2054, 2006.
 S.R. Cloude and K.P. Papathanassiou, "Polarimetric SAR Interferometry," *Geoscience and Remote Sensing, IEEE Transactions on*, vol. 36, no. 5, pp. 1551-1565, 1998.

Optimum Coherence Formulation

Casting the solution for \bar{w}_1 and \bar{w}_2 in a Lagrangian maximization framework, they are solved for in an optimal sense (analytic, closed-form)

$$L = \bar{w}_1^H \mathbf{\Omega} \bar{w}_2 + \lambda_1 (\bar{w}_1^H \mathbf{T}_1 \bar{w}_1) + \lambda_2 (\bar{w}_2^H \mathbf{T}_2 \bar{w}_2)$$

Maximize this term...

$$v = \lambda_1 \lambda_2^*$$

$$\mathbf{T}_2^{-1} \mathbf{\Omega}^H \mathbf{T}_1^{-1} \mathbf{\Omega} \bar{w}_2 = v \bar{w}_2$$

$$\mathbf{T}_1^{-1} \mathbf{\Omega} \mathbf{T}_2^{-1} \mathbf{\Omega}^H \bar{w}_1 = v \bar{w}_1$$

...Solution of eigenvalue problem...

Two sets of three complex eigenvectors and three real non-negative eigenvalues, v_i , are produced in the solution, with the following property:

$$0 \leq v_3 \leq v_2 \leq v_1 \leq 1$$

Magnitudes of the three resulting coherence solutions, $\tilde{\gamma}_i$, are related to the resulting eigenvalues:

$$|\tilde{\gamma}_i| = \sqrt{v_i}$$

Optimum Coherence Products

Change Indication Maps:

$$|\tilde{\gamma}_i| = \sqrt{v_i}, \quad 0 \leq |\tilde{\gamma}_3| \leq |\tilde{\gamma}_2| \leq |\tilde{\gamma}_1| \leq 1$$

Interferograms:

$$\psi = \angle v_i, \quad -\pi \leq \psi \leq \pi$$

Steering Vectors:

$$\bar{w}_{1,1}, \bar{w}_{1,2}, \bar{w}_{1,3}, \bar{w}_{2,1}, \bar{w}_{2,2}, \bar{w}_{2,3}, \quad \|\bar{w}_{i,j}\| = 1$$

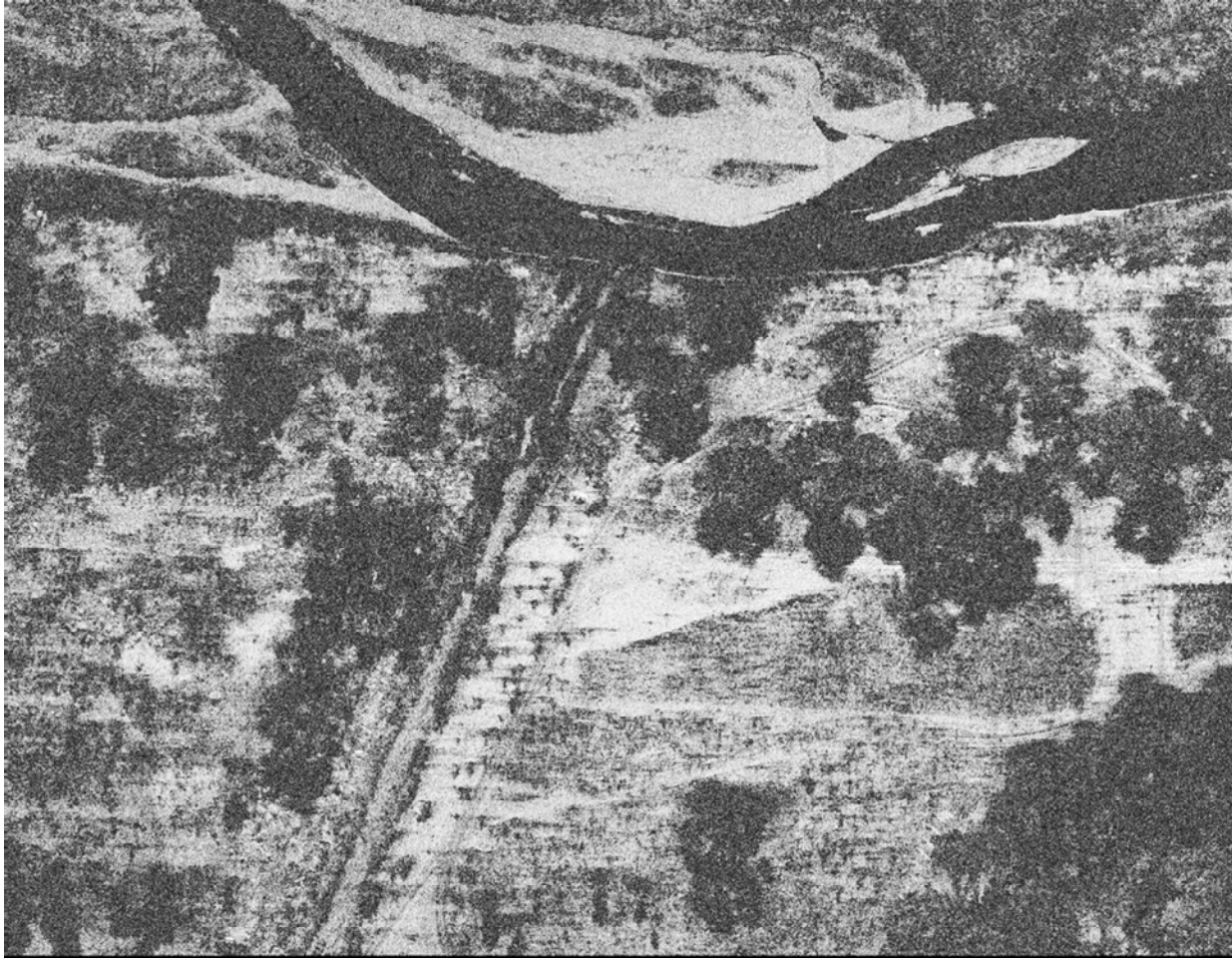
The steering vectors utilize the same Pauli feature bases as the \bar{k} vectors. Hence, these steering vectors can also be decomposed into scattering parameters.

$$\bar{w}_{i,j} = \begin{bmatrix} a \\ b \\ c \end{bmatrix} \begin{array}{l} \rightarrow \text{Weight for odd bounce coherence, surface} \\ \rightarrow \text{Weight for even bounce coherence, } 0^\circ / 90^\circ \text{ di-plane} \\ \rightarrow \text{Weight for even bounce coherence, } \pm 45^\circ \text{ di-plane} \end{array}$$

**APPLICATION:
POLARIMETRIC SAR
CHANGE DISCRIMINATION**

Change Discrimination

The original measured scattering matrices, along with the steering vectors generated from the optimal coherence process, can be utilized to discriminate different types of change within a CCD image.



What types of changes are in a CCD image?

Trees (TRE)

Low-Return (LRT) (radar shadow and the river)

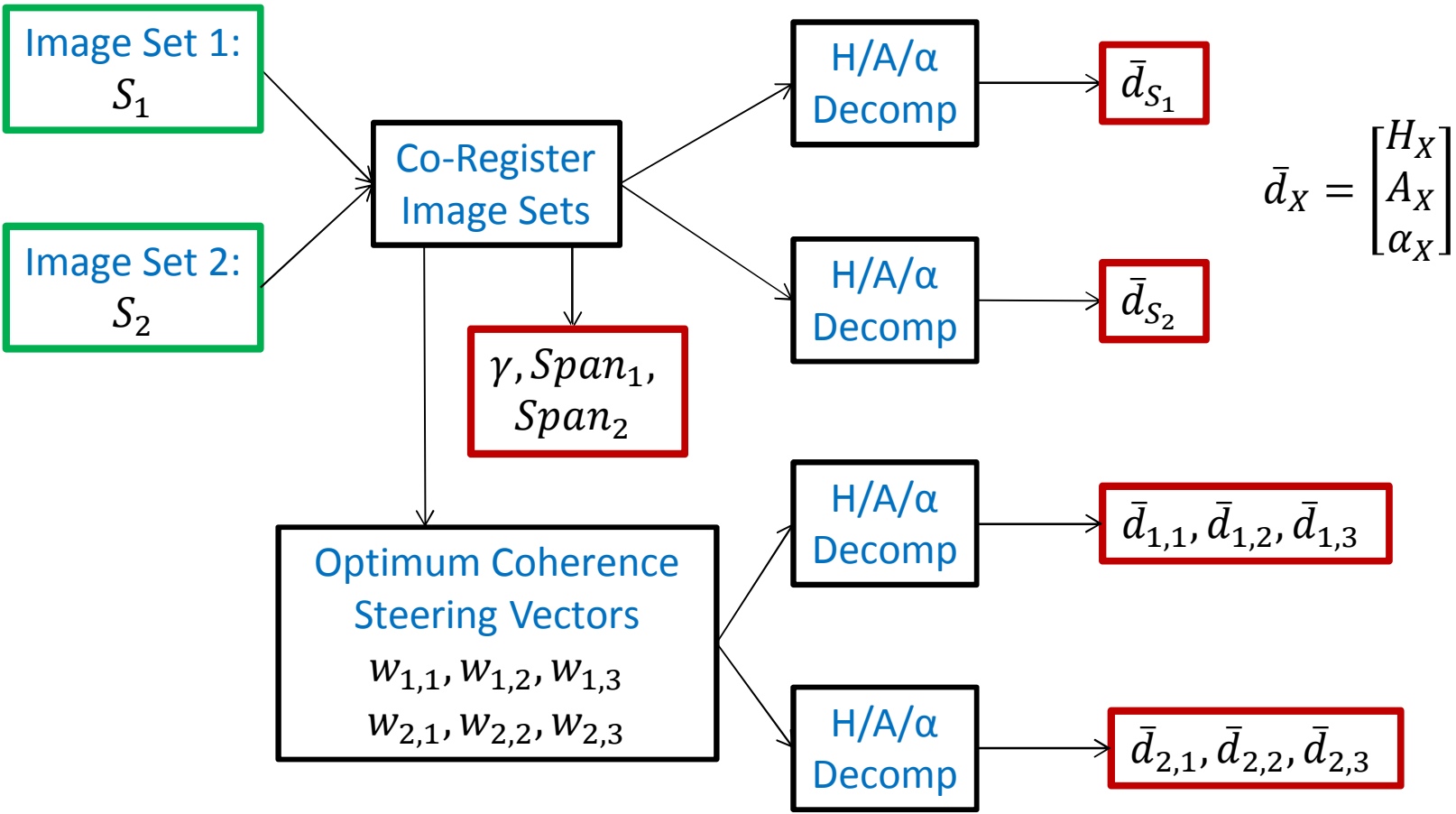
Ground (GRD)

Data Components to Change Discrimination

The following data can be utilized to discriminate between different types of changes in CCD images:

- The H/A/ α values computed from the measured radar values from the first and second passes
- The H/A/ α values computed from all the optimum coherence steering vectors
- The total power (Span) values from the first and second passes
- The CCD values from a given polarization channel

Change Discrimination Framework

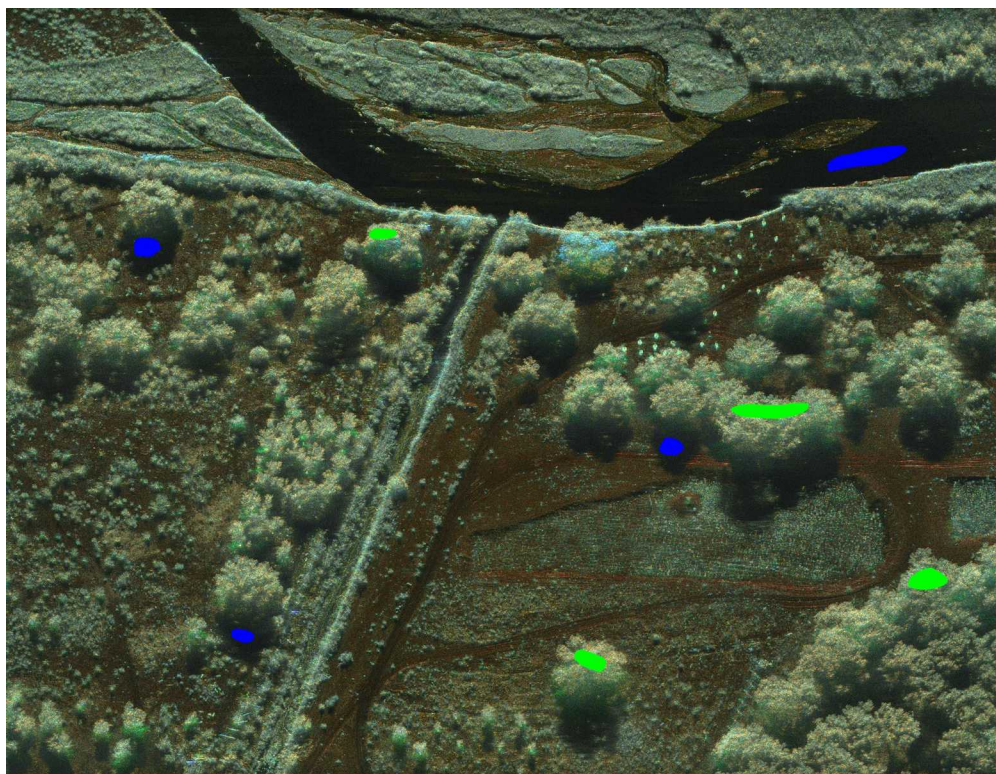


Feature Vector: $\bar{d} = [\bar{d}_{S_1}^T \ \bar{d}_{S_2}^T \ \bar{d}_{1,1}^T \ \bar{d}_{1,2}^T \ \bar{d}_{1,3}^T \ \bar{d}_{2,1}^T \ \bar{d}_{2,2}^T \ \bar{d}_{2,3}^T \ \gamma \ Span_1 \ Span_2]^T$

Change-Type Classes and Data

Models can be built from training data that can discriminate between different types of changes.

Training data were selected from 9 image PolSAR image sets and test data from 6 image sets.



Data for three classes of change-types:

Change-Type	Training Samples	Test Samples
TRE	97,862	73,098
LRT	106,169	75,874
GRD	5,816	5,763

H/A/ α Filter Banks

One approach is to construct H/A/ α filter banks from the training data that can be implemented by way of look-up tables (LUTs)

Training:

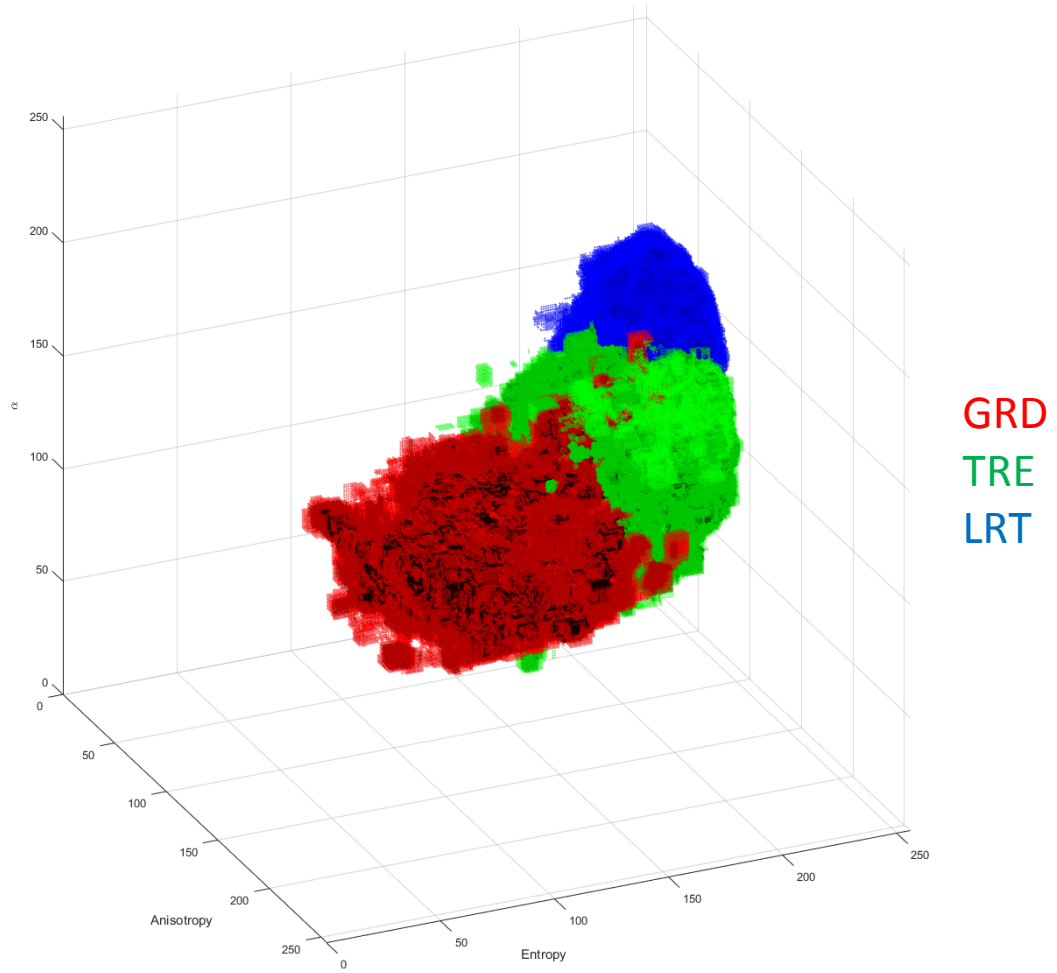
1. Gather training data for a change type of interest
2. Construct filters from normalized 3-D histograms of the sub-vectors, \mathbf{d}_X :
 - a. H/A/ α filters for: $\mathbf{d}_{S_1}, \mathbf{d}_{S_2}, \mathbf{d}_{w_{1,1}}, \mathbf{d}_{w_{1,2}}, \mathbf{d}_{w_{1,3}}, \mathbf{d}_{w_{2,1}}, \mathbf{d}_{w_{2,2}}, \mathbf{d}_{w_{2,3}}$
 - b. Construct additional filter for: $\text{Span}_1, \text{Span}_2, \gamma$

Test:

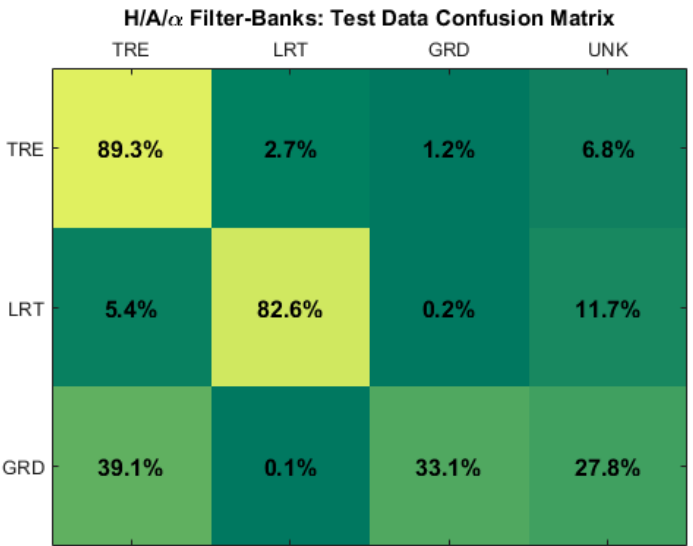
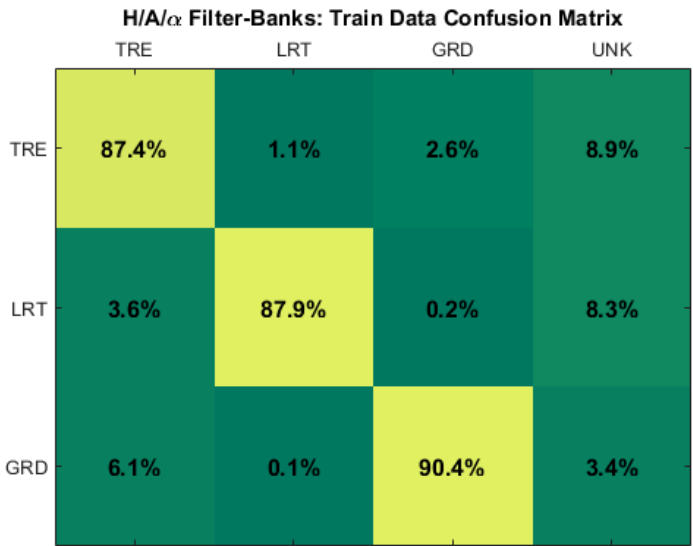
1. Pass feature vectors through filters: $F_X = HA\alpha_X(\mathbf{d}_X)$
2. Evaluate function to determine in-class change type:

$$\gamma_{\text{Changed}} = 1 - (1 - \gamma) \left(\prod_{i=1}^9 F_{X_i} \right)^{\frac{1}{9}}$$

Example S_1 H/A/ α Filter Banks



H/A/ α Filter Banks Confusion

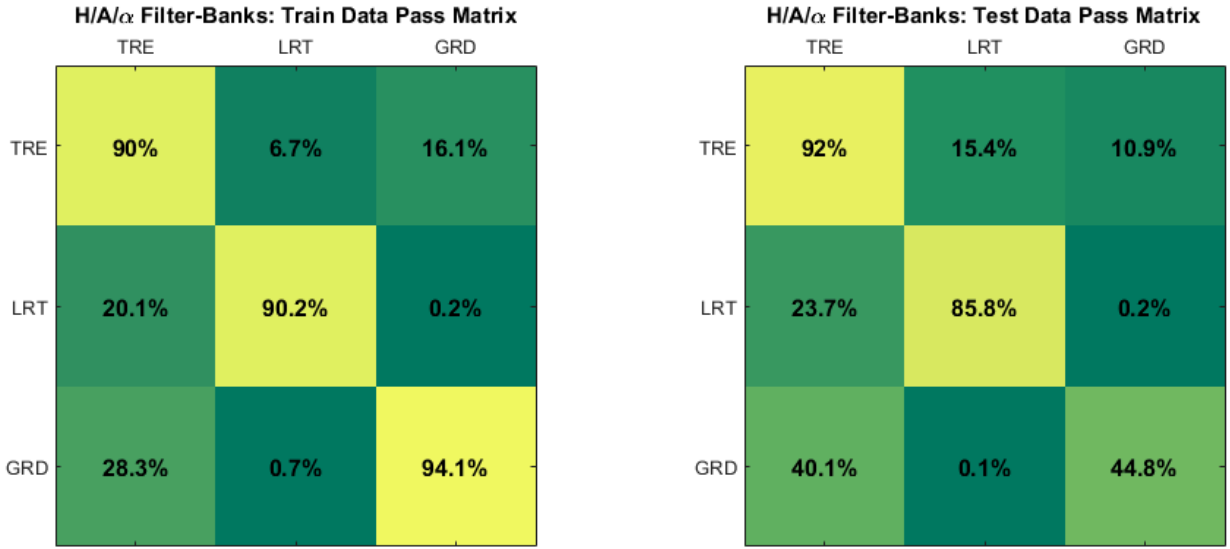


The H/A/ α filters, for each class, were trained on 2,500 samples.

The empiric PD = 90% threshold for the unknown class was determined from a dis-joint set of 2,500 training samples.

The TRE and LRT models generalize well from the training data to the blind test data.

H/A/ α Filter Banks Pass Matrices



Pass matrices illustrate how well the models generalize to blind test data.

The entries correspond to the percentage of in-class and out-of-class samples that are above a given PD threshold for each class.

Ideally, the diagonal of a pass matrix will be the given PD percentage and the off-diagonal elements will be zero.

VV CCD Image -> TRE Change Image



VV CCD Image -> LRT Change Image



VV CCD Image -> GRD Change Image



VV CCD Image -> Confusion Image (PD = 95%)



-  Tree
-  Low-Return
-  Ground
-  Unknown

Future Research in Change Detection

Do the data, for a given type of change, live on a smaller dimensional manifold embedded in the larger ambient space? Can dimension reduction techniques be employed?

Are there other feature vector formulations that are more appropriate for discriminating change types?

H/A/ α filters are one approach to change discrimination, we have tried others as well. How do machine learning techniques compare?

**Thank you for the invitation to
present!!!**

Questions?